Supporting Information for "A Deep Catalogue of Marsquakes"

Nikolaj L. Dahmen[1*], John F. Clinton[2], Men-Andrin Meier[1], Simon C. Stähler[1], Savas Ceylan[1], Doyeon Kim[1], Alexander E. Stott[3], and Domenico Giardini[1]

[1]Institute of Geophysics, ETH Zurich, Zurich, Switzerland
[2]Swiss Seismological Service, ETH Zurich, Zurich, Switzerland
[2]Institut Supérieur de l'Aéronautique et de l'Espace SUPAERO, Toulouse, France

Contents of this file

1. Figures S1: overview of Marsquake Service catalogue and noise evolution
2. Figure S2-S5: details on model selection and optimisation; synthetic examples
3. Figure S6-14: review of new detection
4. Figure S15-16: low frequency event family rate and temporal distribution of all detections across mission

Additional Supporting Information (Files uploaded separately)

1. Extended catalogue as csv.file (MQNet_DeepCatalogue.csv)
   and QUAKEML-file (MQNet_DeepCatalogue.xml), with:
   - event name
   - start&end time of detection
   - event family
   - sol of occurrence
   - Boolean indicating whether detection score above/below detection threshold
   - detection value
   - denoised 90th percentile amplitudes in low- and high frequency bands
   - model used in detection
   - comment with manual determined event type
2. Summary of all detections above detection threshold (MQNet_AllDetections.csv):
3. Sol-wise event masks for Sol 182-1224 with new detections and MQS events, following Fig. 7 (b) (MQNet_Predictions.pdf)

*Correspondence to `nikolaj.dahmen@erdw.ethz.ch`

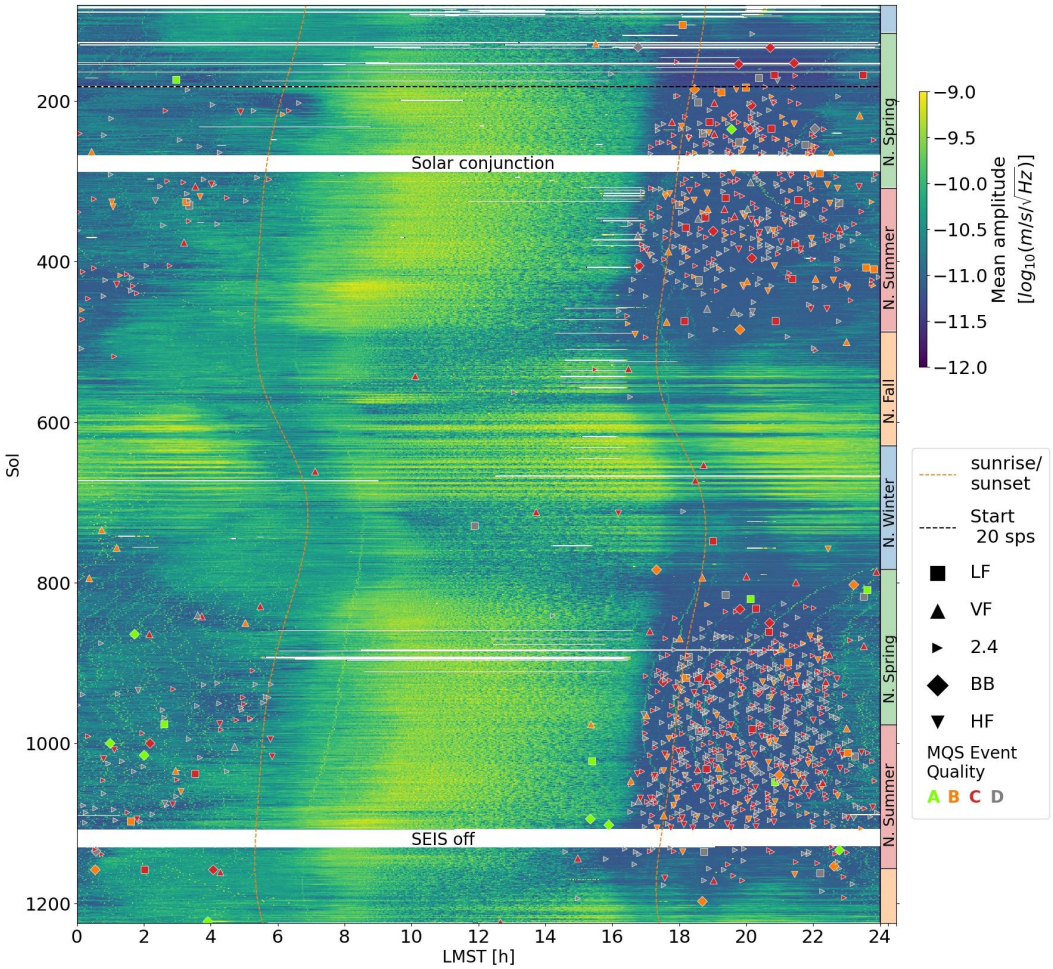

Figure S1: Overview of MQS catalogue and noise variations (Sol 80-1222). The background represents the mean noise level of the vertical component between 0.1-4.5 Hz computed from the 10&20 sps channels (switch to continuous 20 sps data on Sol 182). Martian seasons on Northern hemisphere are indicated on the right. All events in the MQS catalogue are indicated with their quality (A-D) and event type: low frequency (LF), broadband (BB), 2.4 Hz (2.4), high frequency (HF), very high frequency (VF). LMST: local mean solar time; MQS: Marsquake Service; SEIS: Seismic Experiment for Interior Structure.

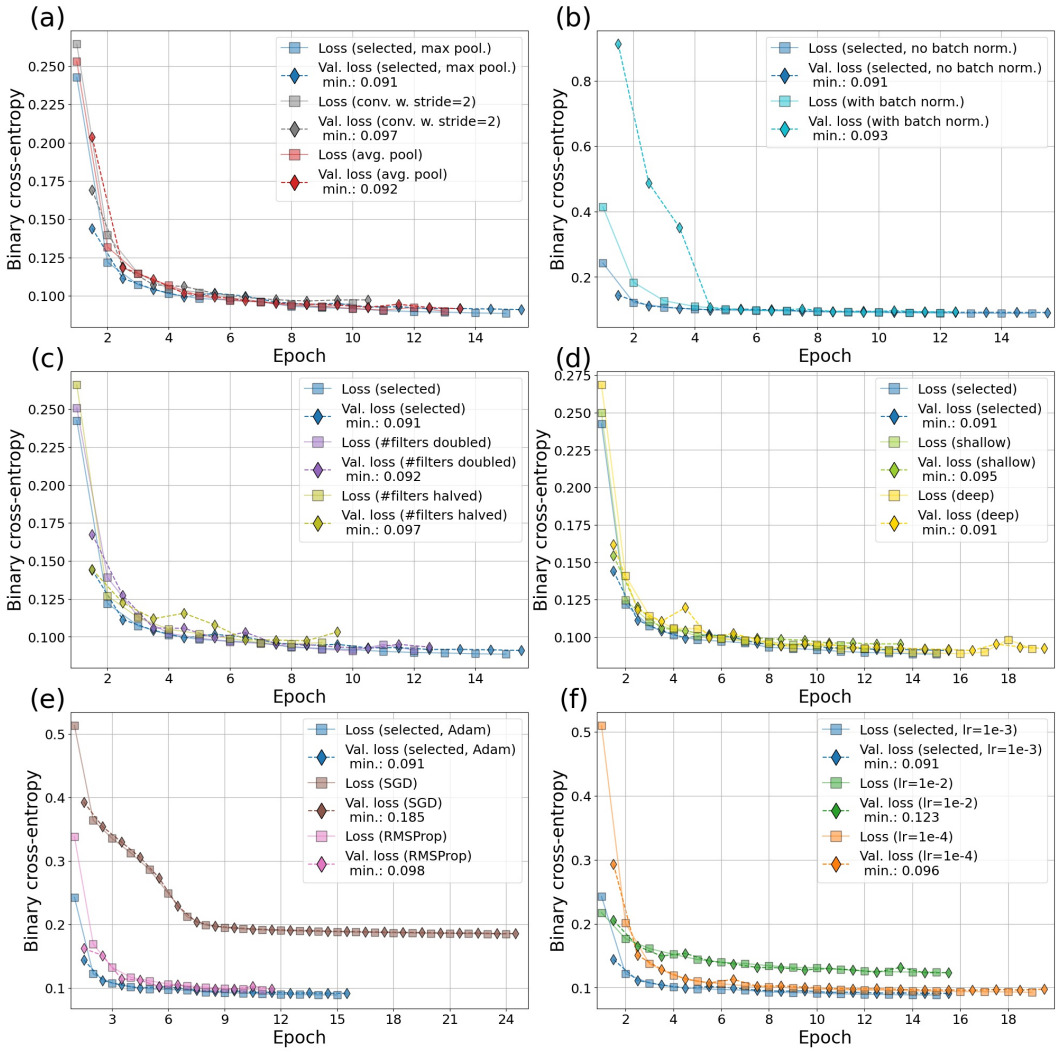

Figure S2: Overview of other tested models. Shown are the training and validation loss on a smaller subset (5k/2.5k samples) for our selected model (blue in each plot) and modifications: (a) down-sampling operation with max pooling (selected model) compared to average pooling or an additional convolutional layer with stride 2; (b) adding batch normalisation layers after each convolutional layer; (c) increasing or reducing the number of filters in each convolutional layer; (d) increasing or reducing the depth of the model; (e) optimisers with default learning rate (lr), namely Adam (lr=0.001), RMSProp (lr=0.001) and vanilla stochastic gradient descent (SGD, lr=0.01); (f) different learning rates for Adam optimiser. The training is stopped after 3 epochs without improvement, and the minimum loss on the validation set is reported. Several tested modifications perform similarly well as the selected model (e.g. with average pooling layer, batch normalisation layers), though some of them are much larger and take longer in training than the selected model (higher number of filters, deeper model). Note that the validation loss curves are offset to the right.

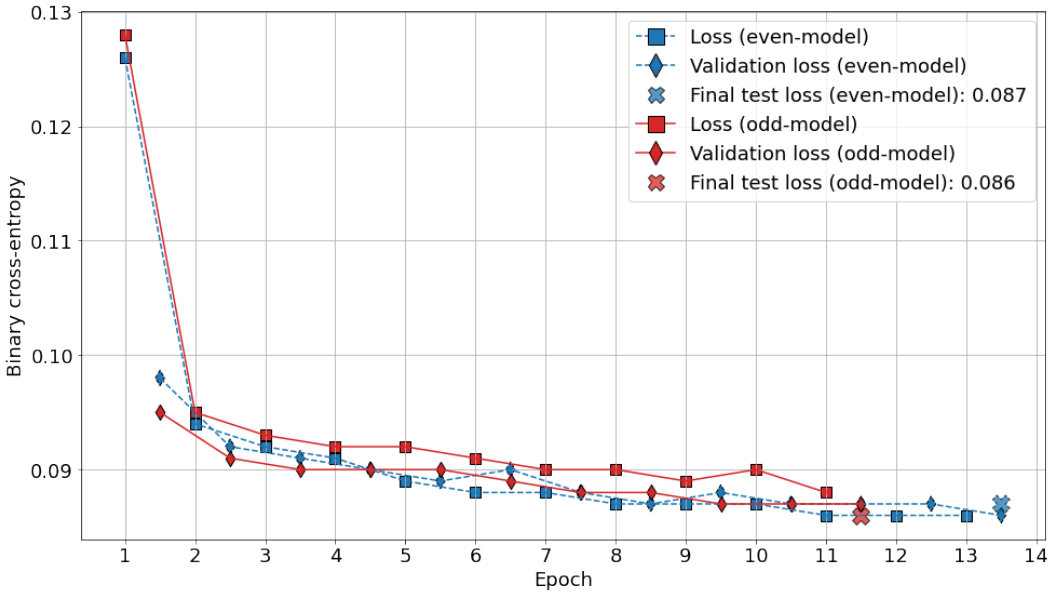

Figure S3: Loss during training. Training and validation loss (binary cross-entropy) for models trained on noise from even&odd-sol numbers. Final test loss is computed on odd-number validation set for even-number model, and vice versa, for odd-number model. Note that the validation loss curves are offset to the right.

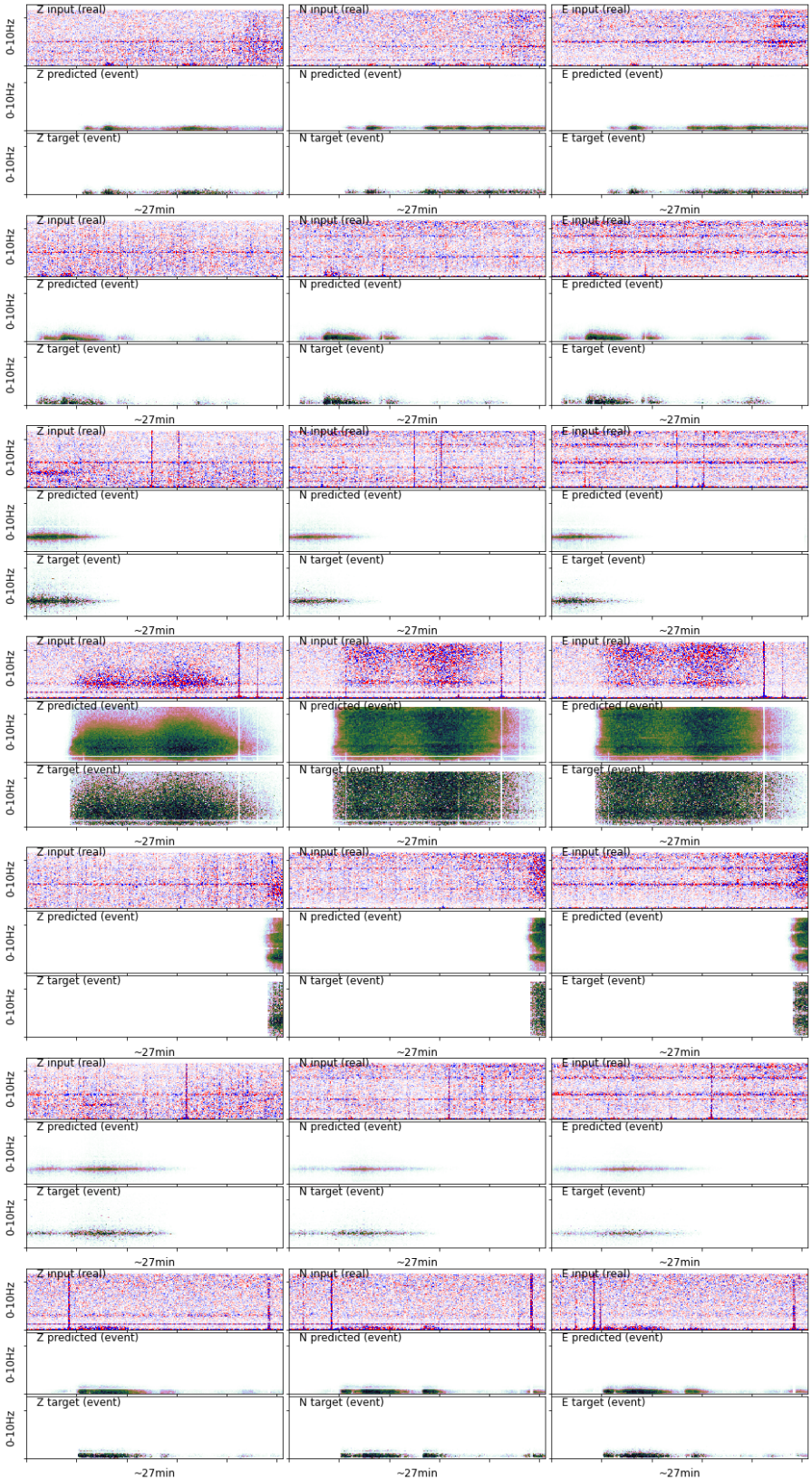

Figure S4: Prediction on synthetic test dataset. Seven synthetic events recordings (represented by real part of STFT), predicted event masks and target event masks for ZNE components. STFT: short-time Fourier transformation.

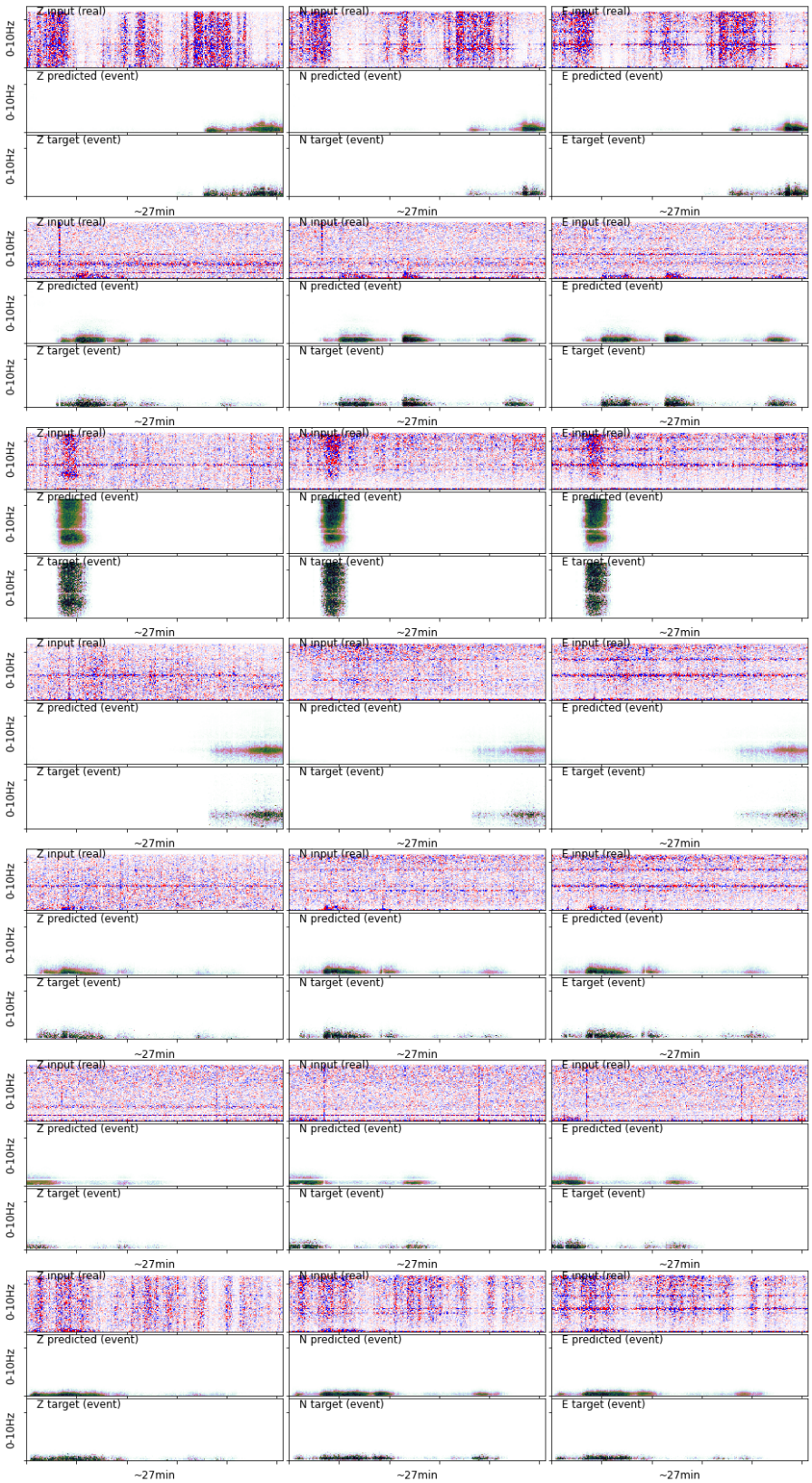

Figure S5: Prediction on synthetic test dataset. Seven synthetic events recordings (represented by real part of STFT), predicted event masks and target event masks for ZNE components. STFT: short-time Fourier transformation.

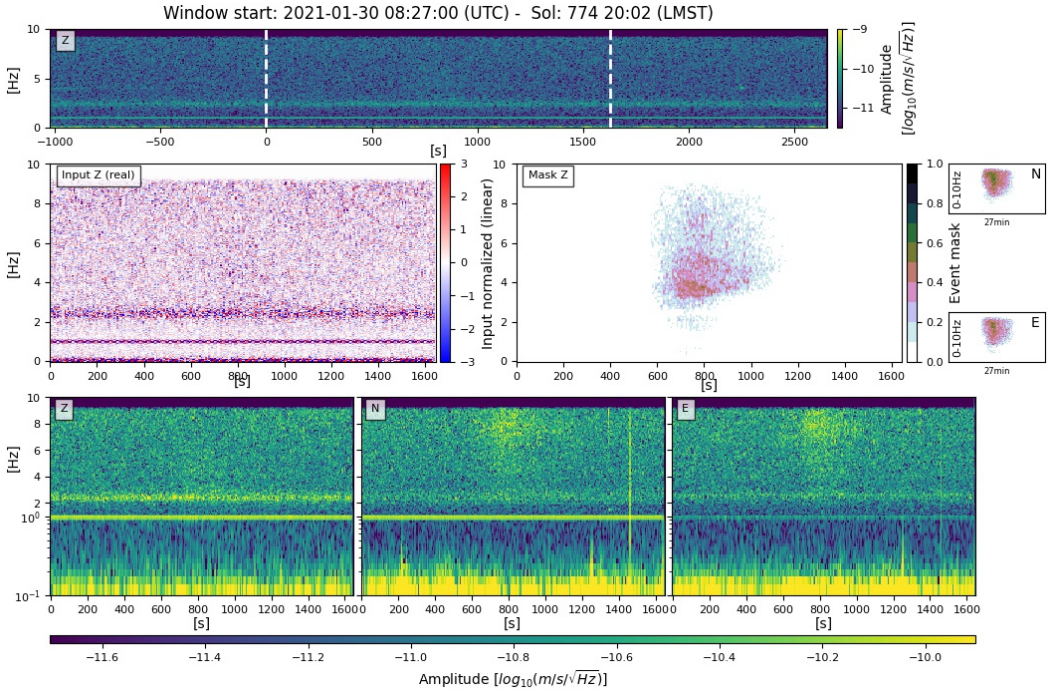

Figure S6: Overview plot of new VF detection (D0774a). The top plot shows a wide window of the vertical component spectrogram, with the white dashed lines indicating the time window shown in all other plots. Middle left plot shows the model input (real part, Z component) and right side show the model output (event mask, Z), as well the output for the horizontal components in small plots. The bottom row shows the three components with an adjusted color bar. Indicative for the VF event is the high frequency energy (>6 Hz) on the horizontal components, and the absence of any lander mode excitation that would otherwise suggest a wind gust (similar to S1048f, Fig. 6).

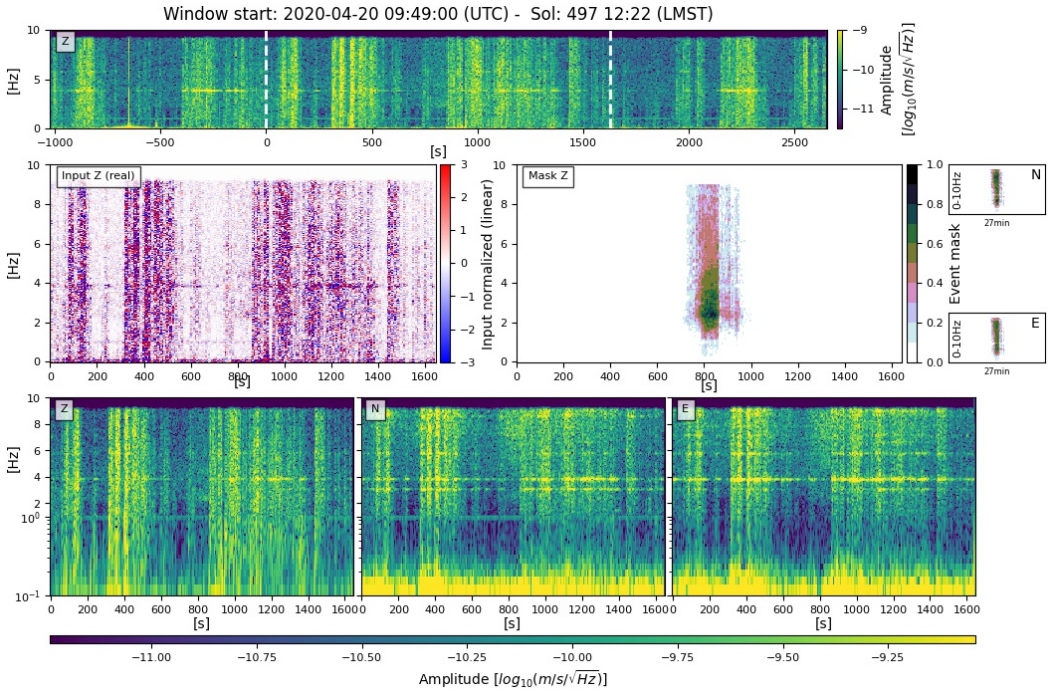

Figure S7: Overview plot of new VF detection (D0497a), following Figure S6. The event is visible in the short quiet period in between the wind gusts: the vertical component shows 2.4 Hz energy and horizontal components indicates energy at high frequencies (>6 Hz), characteristic for VF events. While the lander modes are strongly excited before and after the events, they show no or little excitation during the event (similar to S0712a, Fig. 6).

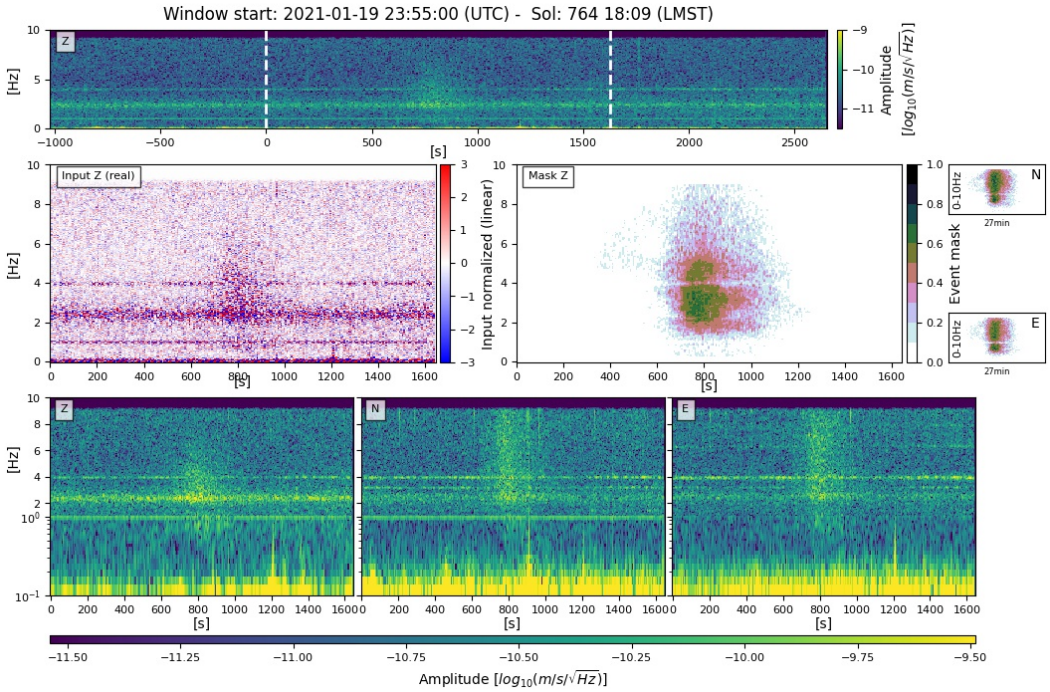

Figure S8: Overview plot of new VF detection (D0764a), following Figure S6. This detection is during a relative quiet period but with high ambient 2.4 Hz excitation. The VF event is clearly visible with 2.4 Hz energy and high frequency (>6 Hz) energy on the horizontal components.

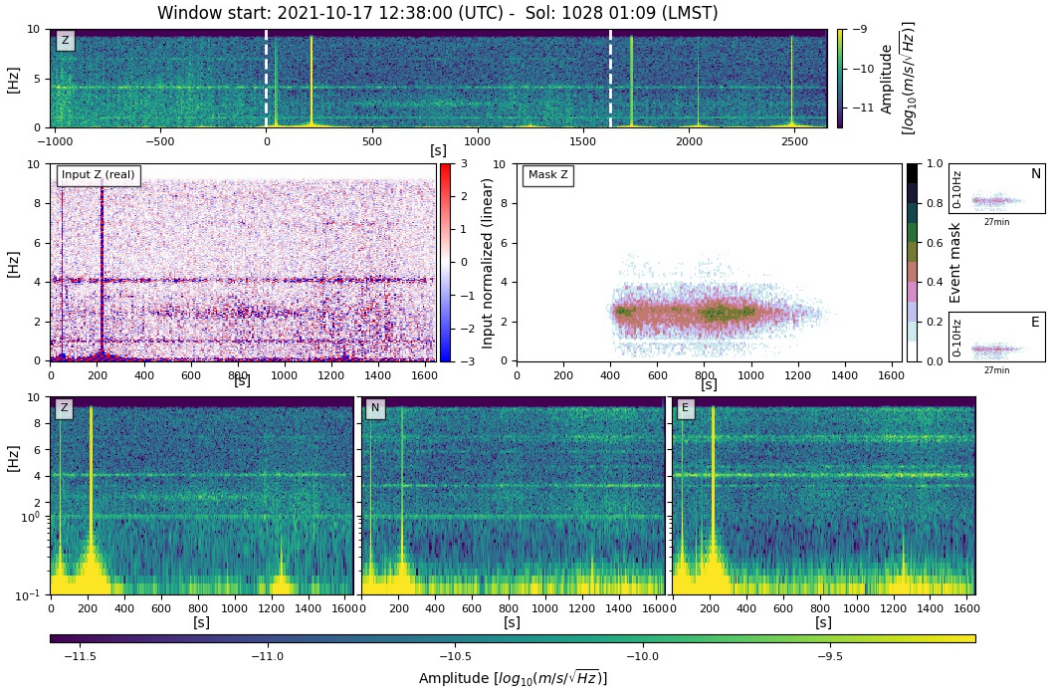

Figure S9: Overview plot of new 2.4 Hz/HF detection (D1028a), following Figure S6. The detection is made during a noisier period (indicated by lander mode excitation). We see clear 2.4 Hz energy (mainly on vertical component) that is characteristic for 2.4/HF events (compare Figs. 2 and 6).

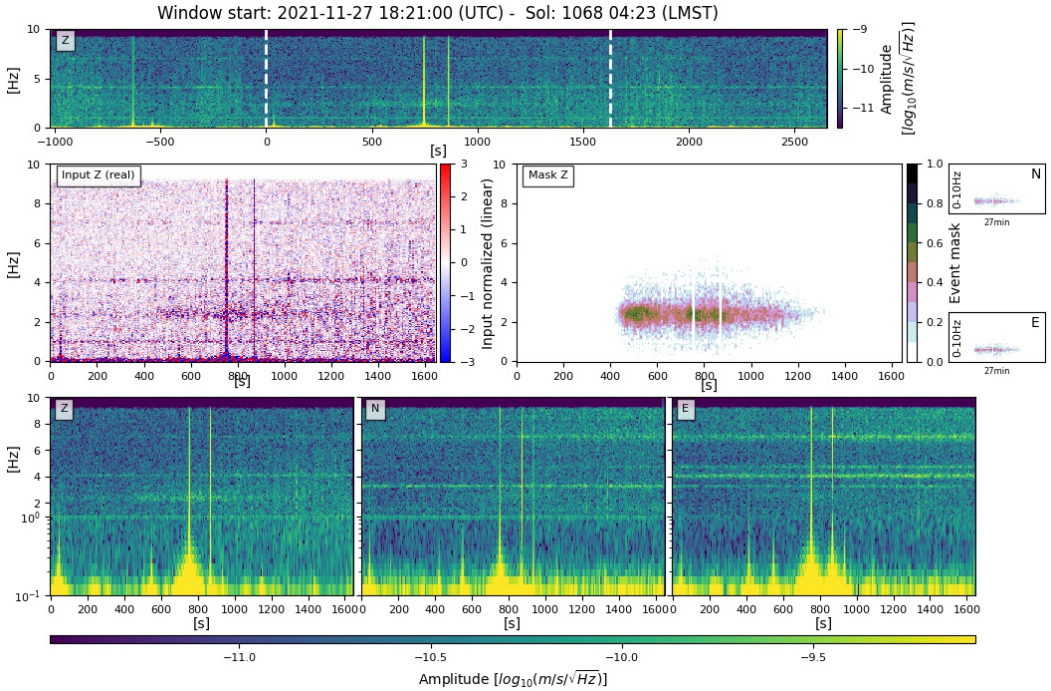

Figure S10: Overview plot of new 2.4 Hz/HF detection (D1068b), following Figure S6. The detection is similar to Figure S9; additionally corrupted by two large glitches during event.

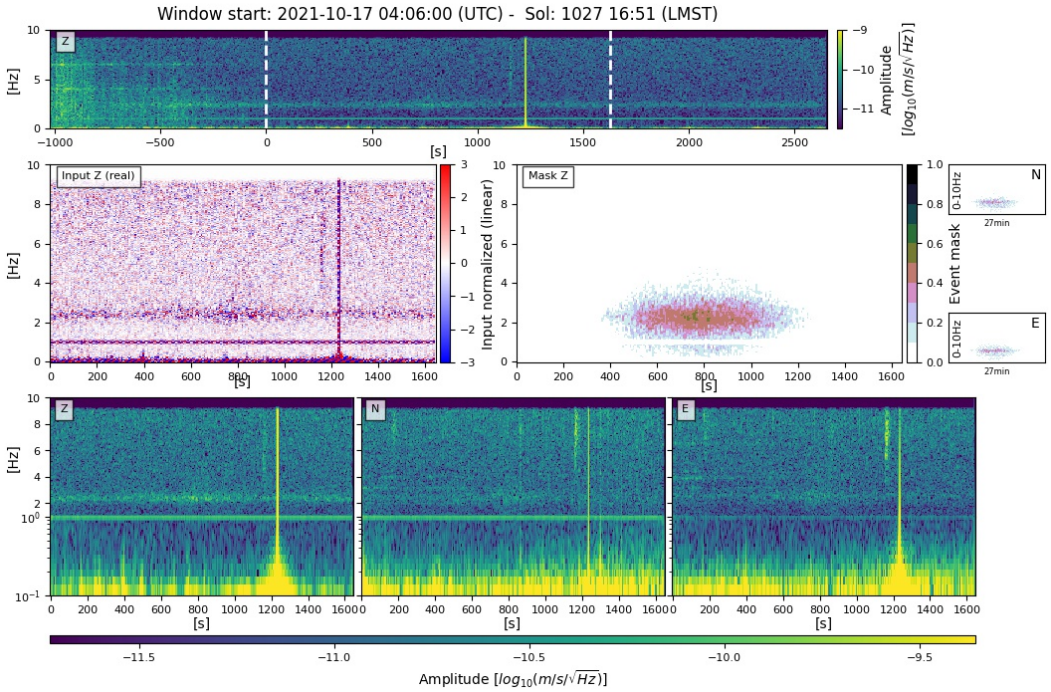

Figure S11: Overview plot of new 2.4 Hz/HF detection (D1027c), following Figure S6. A weak event during quiet period with characteristic 2.4/HF energy.

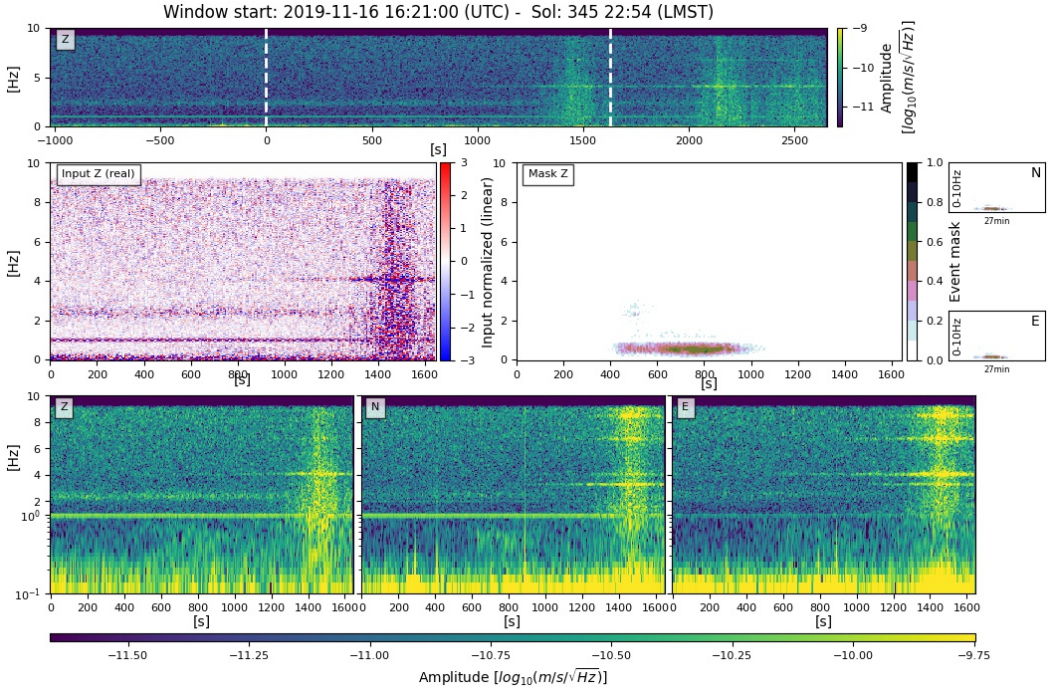

Figure S12: Overview plot of new LF detection (D0345a), following Figure S6. Indicative for the LF event is the the typical low frequency energy that is not explained by wind noise (see lander modes that are excited later by wind.). Compare Figs. 2 and 6.

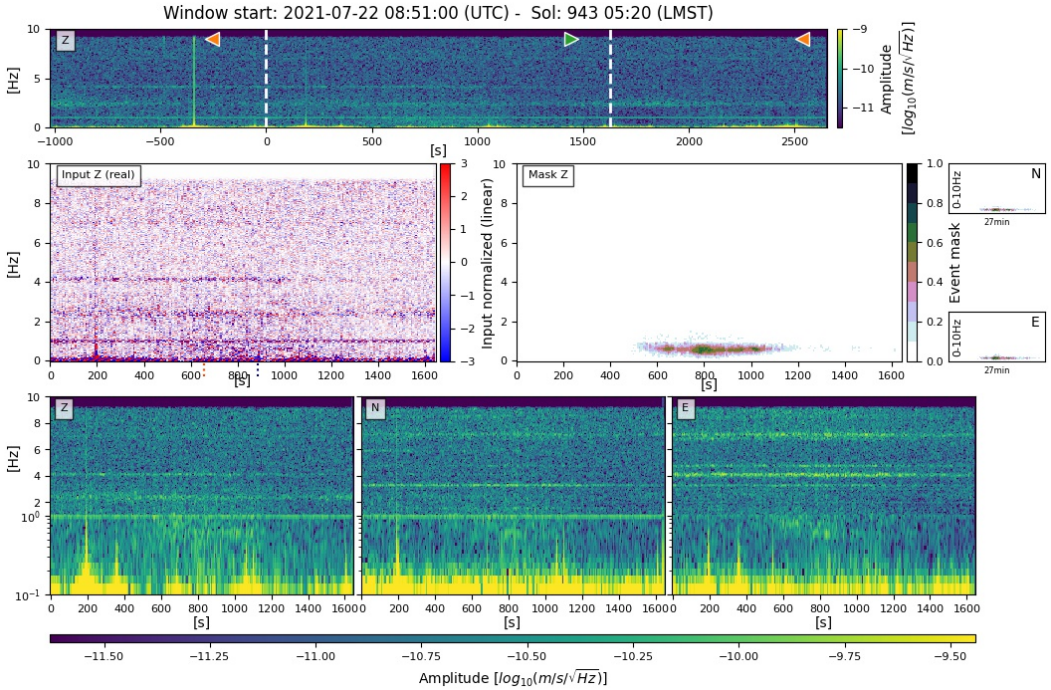

Figure S13: Overview plot of new LF detection (D0943a), following Figure S6. The potential LF event occurred during noisier period and is identified by low-frequency energy that is not explained by wind noise (lander modes are continuously excited). Compare Figs. 2 and 6).

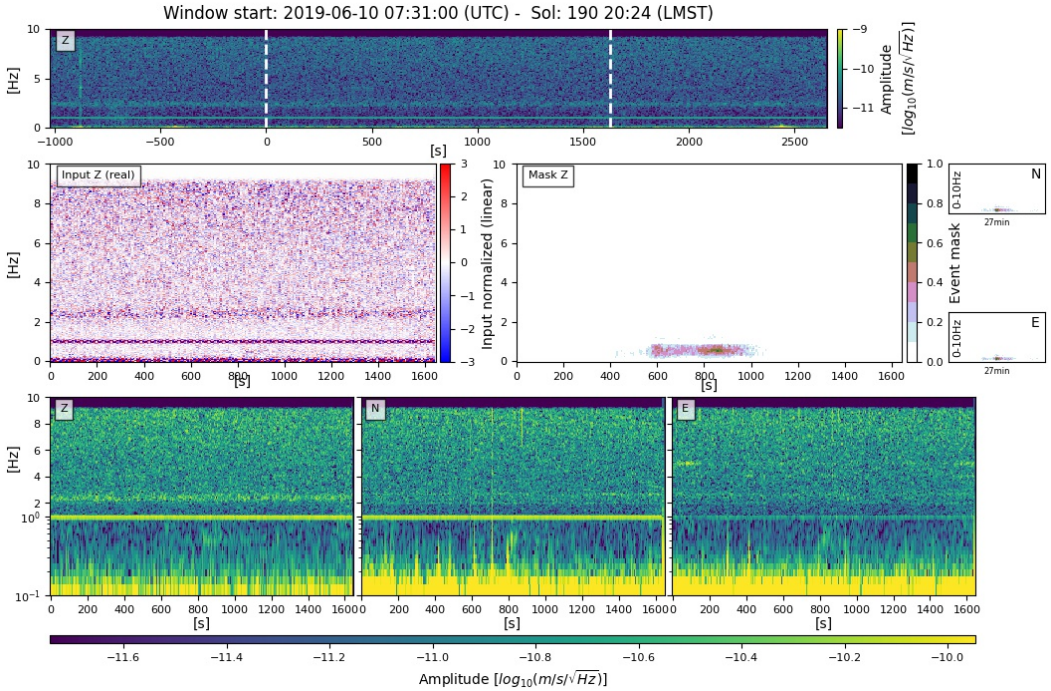

Figure S14: Overview plot of new LF detection (D0190a), following Figure S6, LF event is indicated by low frequency energy, similar to Figure S12.

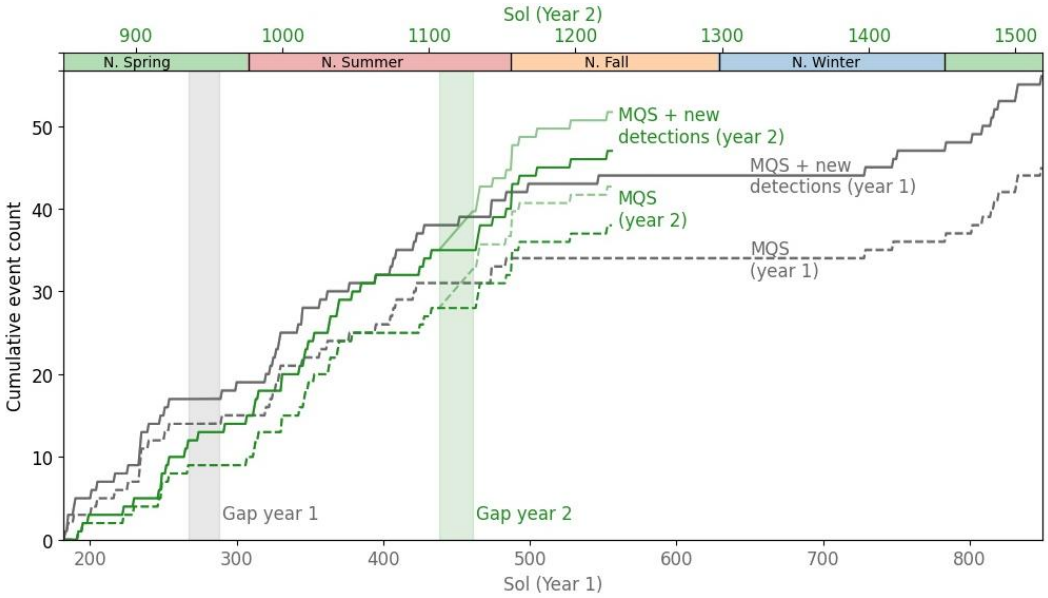

Figure S15: Cumulative event count for LF family events. Shown are the cumulative event number of all new detections (above detection threshold) and MQS events for first (solid-grey line, Sol 182-850) and second Martian year (solid-green line, from Sol 850); dashed lines show numbers from MQS catalogue alone. Faint-coloured lines include an estimate of the event numbers during the gaps in the first and second year. LF: low frequency; MQS: Marsquake Service.

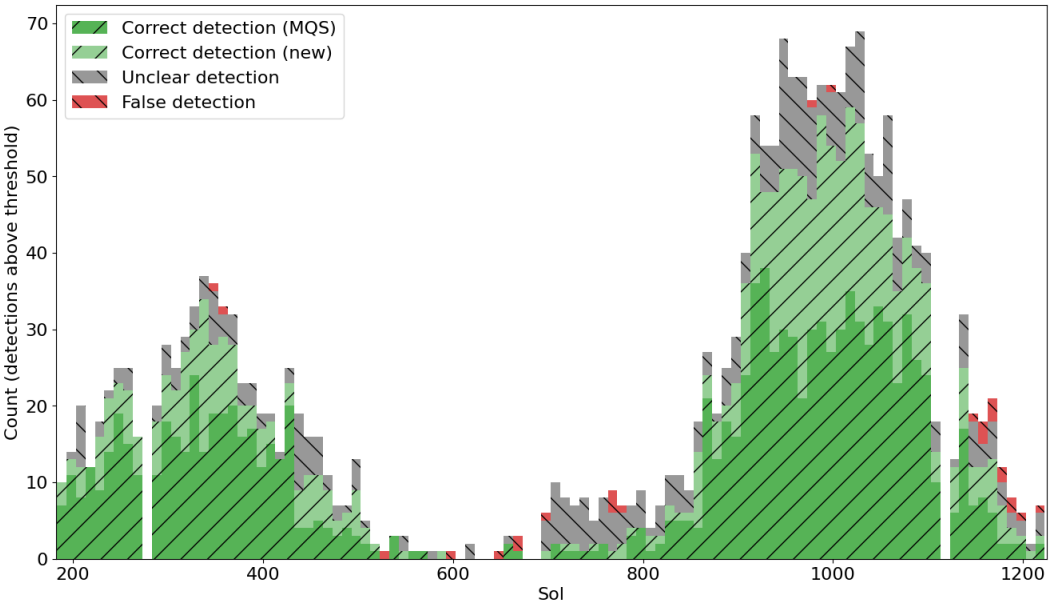

Figure S16: Detections across the mission. Correct detections (both matching MQS events and new) mainly fall in spring and summer of the first and second Martian year. Unclear detections follow a similar distribution, but additionally contain a (relatively) high number around Sol 700-800. The histogram bins are approx. 10 sols wide. MQS: Marsquake Service.